Production d'énergie (hydraulique, thermique et nucléaire)

SIMULATION NUMERIQUE DIRECTE DE CONVECTION LIBRE DANS UN CANAL VERTICAL : UN OUTIL POUR LA MODELISATION DE LA TURBULENCE AU SECOND ORDRE

DIRECT NUMERICAL SIMULATION OF FREE CONVECTION IN A VERTICAL CHANNEL : A TOOL FOR SECOND MOMENT CLOSURE MODELING

Direction des Etudes et Recherches

EDF
Electricité de France

Direction des Etudes et Recherches

SERVICE APPLICATIONS DE L'ELECTRICITE ET ENVIRONNEMENT
Département Laboratoire National d'Hydraulique

Mars 1996

BOUDJEMADI R.
MAUPU V.
LAURENCE D.
LE QUERE P.

SIMULATION NUMERIQUE DIRECTE DE CONVECTION LIBRE DANS UN CANAL VERTICAL : UN OUTIL POUR LA MODELISATION DE LA TURBULENCE AU SECOND ORDRE

DIRECT NUMERICAL SIMULATION OF FREE CONVECTION IN A VERTICAL CHANNEL : A TOOL FOR SECOND MOMENT CLOSURE MODELING

Pages : 14

96NB00158

Diffusion : J.-M. Lecœuvre
EDF-DER
Service IPN. Département SID
1, avenue du Général-de-Gaulle
92141 Clamart Cedex

ISSN 1161-0611

SYNTHÈSE :

On a calculé la convection turbulente naturelle dans une fente verticale infinie à chauffage différentiel à l'aide d'un code mixte Fourier et différences finies. Pour un nombre de Raleigh de 10^5, des perturbations périodiques provenant de la solution laminaire se développent et il se produit une transition vers un régime entièrement turbulent.

A partir de ce moment, on a constitué une base de données des corrélations d'ordre supérieur que l'on a utilisée pour tester une fermeture du second moment basée sur le modèle LRR et la relaxation elliptique pour les effets proches de la paroi. Le transport turbulent à contre gradient apparu dans la partie centrale du canal a nécessité un modèle algébrique pour les triples corrélations au lieu des modèles à diffusion DH ou HL standard.

EXECUTIVE SUMMARY :

Natural turbulent convection in a differentially heated infinite vertical slot is computed with a mixed finite differences/Fourier code. At a Rayleigh number of 10^5, periodic perturbations from the laminar solution develop and transition to a fully turbulent flow occurs.

From then on, a database of high order correlations is constituted and used for testing of a second moment closure based on the LRR model and elliptic relaxation for near wall effects. Counter gradient turbulent transport, found in the central part of the channel, requires an algebraic model for the triple correlations instead of the standard DH or HL gradient diffusion models.

Direct numerical simulation of free convection in a vertical channel : a tool for second moment closure modeling

R. Boudjemadi[b], V. Maupu[a], D. Laurence[a], and P. Le Quéré[b]

[a] EDF Laboratoire National d'Hydraulique, B.P. 49, 78401 Chatou Cedex, France

[b] LIMSI, CNRS, BP 133, 91403 Orsay Cedex, France

1. INTRODUCTION

Much progress has been achieved in realistic modelling of unknown dynamic terms in one point closure models (Launder et al. [1], Durbin [2], Lumley [3]) thanks to databases obtained from Direct Numerical Simulations. Less data is available concerning turbulent heat fluxes, with the notable exceptions of Kasagi et al. [4] and Lyons et al. [5]. Even less is known about the budgets of these moments in the natural convection case. Indeed, simulations are solely available in transitional regimes (Henkes [6]) probably because many natural convection situations include stratification effects so that fully turbulent simulations require higher Ra numbers and consequently very high grid resolution.

Natural convection flow is split in two main categories, the first in which the horizontal plates are heated differently, the thermal gradient vector being parallel to the gravity vector, and the second in which vertical walls are differentialy heated. In this case considered here, the physics of the flow in finite cavities can be relatively complex including many physical phenomena (stratification, hydraulic jump, boundary layer). The problem is simplified (numerically but not experimentally!) by studying the flow in infinite vertical deep slot. We separate again two different regimes (Fig. 1 and 2) :

a) the conduction solution (without stratification, an experimental challenge!),

b) the double boundary layer solution (with stratification).

Because most practical situations are characterized by some stratification, simulations of the double buoyancy layer would seem more relevant. However, as shown by previous 2D simulations (Xin [7]) and confirmed by the present work (Boudjemadi [8]), it appears very difficult to obtain reliable chaotic solutions, we

decided to first perform direct simulations starting from the conduction solution.

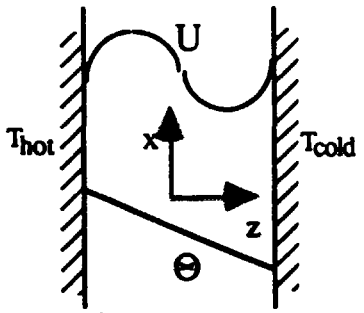

Figure 1 : Conduction state configuration (without stratification).

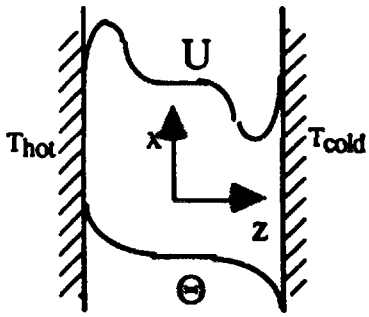

Figure 2 : Double boundary layer configuration (with stratification).

2. DIRECT NUMERICAL SIMULATIONS

2.1 configuration and governing equations

We consider an incompressible flow where the motion is induced by gravity forces. This phenomenon is assumed to be governed by the three-dimensional equations of Boussinesq. The equations are written and integrated as perturbations from the laminar pure conduction solution or "basic solution" (U_i^b, θ^b). Thus source terms expressed from gradients of the (given) basic solution appear in the perturbation equations for velocity and temperature (u_i, θ).

$$\begin{cases} u_{i,i} = 0 \\ u_{i,t} + (u_j + U_j^b)u_{i,j} = -\dfrac{1}{\rho_0} p_{,i} + \left(\nu u_{i,j}\right)_{,j} + g_i \beta\theta - u_j U_{i,j}^b \\ \theta_{,t} + (u_j + U_j^b)\theta_{,j} = \left(\kappa\theta_{,j}\right)_{,j} - u_j \Theta_{,j}^b \end{cases} \tag{1}$$

The exact non-dimensional basic solutions of the conduction regime are given by Vest & Arpaci [9]. For vertical walls at z=-0.5 and z=0.5 they read:

$$\begin{cases} U_1^b(z) = U^b(z) = 1/6z(z-1/2)(z+1/2) \text{ and } U_2^b(z) = U_3^b(z) = 0 \\ \theta^b(z) = -z \end{cases} \tag{2}$$

The reference quantities for the non-dimensional Boussinesq equations, are L_{ref} =D, standing for the gap width, $U_{ref} = g\beta\Delta T D^2/\nu$ for velocity, L_{ref} / U_{ref} for time and ΔT for temperature. (g, β, ΔT, ν are respectively the gravity, the dilatation parameter, the temperature difference between walls and the kinematic viscosity). The non-dimensional system is thus:

$$\begin{cases} u_{i,i} = 0 \\ u_{i,t} + (u_j + U_j^b)u_{i,j} = -\dfrac{1}{\rho_0} p_{,i} + \left(\dfrac{1}{Gr} u_{i,j}\right)_{,j} + \dfrac{1}{Gr}\theta\delta_{i1} - u_j U_{i,j}^b \\ \theta_{,t} + (u_j + U_j^b)\theta_{,j} = \left(\dfrac{1}{Ra}\theta_{,j}\right)_{,j} - u_j \Theta_{,j}^b \end{cases} \tag{3}$$

with $Ra = \frac{g\beta\Delta TD^3}{\nu\kappa}$ (Rayleigh number), and $Gr = \frac{g\beta\Delta TD^3}{\nu^2}$ (Grashof number)

Here i, j = 1,2,3 correspond to x, y, z respectively, where x, y and z are respectively the streamwise (vertical), spanwise, and normal coordinates. δ_{ij} is the Kronecker symbol.

2.1 Numerical method

Following for instance the work of Grötzbach and Wörner [10] in Rayleigh Bénard convection, a mixed spectral/finite difference direct simulation of an active scalar field within a vertical channel flow has been achieved at a Rayleigh number of 10^5 with a molecular Prandtl number of 0.71.
The equations are integrated in time using a 3 fractional step scheme : Convection, Diffusion + Gravity terms + Sources terms, Pressure + Continuity.
Time integration is based on an Adams-Bashforth scheme for the convective step and a Crank-Nicolson scheme for the diffusion one.
Convection is treated in the physical space under semi-conservative (Arakawa) form and discretized in fourth order finite difference while the two other steps are solved after a double Fast Fourier Transform of variables (in the homogeneous directions x and y). Derivatives in the wall to wall direction are then discretized with a standard second order finite difference scheme. Pressure and velocity grid arrangement is staggered. Following Schumann [11], tridiagonal linear systems are then obtained and solved exactly with a mixed Fourier - tridiagonal algorithm.
The coefficient of the standard hyperbolic tangent distribution of nodes in the wall normal direction is set to 0.9, giving a slightly stretched grid.
Natural no slip boundary conditions are given at the wall for the velocity and constant value for the temperature. No pressure boundary condition is required.

2.2 Validation

Validation have been carried out in order to test the ability of the present numerical procedure to simulate the loss of linear stability of firstly, a Poiseuille flow and secondly, a conduction flow. In the first test case,correct eigen functions and growth rate have been recovered while in the latter test case (see Chait and Korpela [12] for details), a misrepresentation of kinetic and potential energy spectrum obtained with a first order time discretisation has led us to use a second order time scheme.
Then, following the approach of Jimenez and Moin [13] and in order to validate the code in turbulent regimes, an isothermal fully turbulent channel flow (Re_τ =160) has been predicted in a restricted computational domain (Lx=2.55, Ly=0.9, Lz=2.0, with a 40x24x129 grid resolution). Statistics are similar to the ones published in [13].

2.3 Methodology

The last computation was a conduction flow at Ra = 10^5. Starting from the basic laminar solution, the computation was initiated with zero perturbations on the velocity field and a random perturbation on the temperature field. Due to gravity, these temperature perturbations lead to vertical velocity fluctuations which, due to the gradients in the basic profiles, rapidly develop into 2D perturbations. After a nondimensional (buoyancy) time of T1=2.7 10^4 (figure 1b), perturbations in the spanwise direction also developed. Dimensions of the

computational domain, and grid size are given in table 1 and have been chosen in order to correctly represent all essential scales of turbulence.

Ra	Mesh	Computation box	Δt
$1\ 10^5$	64x32x65	2.5x1x1	0.9

Table 1 :computational parameters of the $Ra=10^5$ simulation

The statistical averages were started once the time signals of all 3 velocity components seemed to have developed from a quasi-periodic to a fully random state. This corresponds to $T2 = 8.5\ 10^4$ (figure 1d). Special care has been taken to ensure vanishing of two-point velocity correlations for sufficiently large distances and to obtain high quality of velocity and temperature spectra. The integration was continued until $T3 = 2.75\ 10^5$ which was chosen so as to obtain time independent fully (anti)symmetrical profiles. Imbalance of second moment equation budgets were below 1% of the peak of production. The total averaging was thus conducted over a (buoyancy) time interval $T3-T2 = 1.9\ 10^5$.

2.4 DNS results

All following quantities are normalized by u^* and θ^* defined as :

$$u^{*2} = \left|\nu \frac{\partial U}{\partial z}\right|_{wall} \quad \text{and} \quad \theta^* = \frac{1}{u^*}\left|\kappa \frac{\partial \Theta}{\partial z}\right|_{wall} \tag{4}$$

where U and Θ are respectively the mean values of velocity and temperature

Here $u^*/Vref = 4.94\ 10^{-4}$ and $\theta^*/T_{ref} = 5.15\ 10^{-2}$.

Figure 2 shows the mean temperature profile and figure 3 the total heat flux and the mean temperature gradient (which is proportional to molecular heat flux). The wall temperature gradient corresponds to a Nusselt number of $Nu = 2.62$. The total heat flux is equal to unity which confirms a high level of statistical convergence. Figure 4 shows that the vertical heat flux is four times higher than the wall to wall flux, while an eddy diffusivity model would yield a null value for this term since there is no temperature gradient in this direction.

The mean velocity profile shown on figure 5 is composed of a constant gradient region in the center of the channel and a boundary layer. Comparing this with the shear stress profile on figure 6, we notice that in opposition to the velocity gradient, the shear stress does not change sign (which an eddy viscosity model could not reproduce). As can be seen on figure 7, the shear-production term does become negative as expected, but it is overbalanced by the transport term and a weaker effect of the gravity production.

The profiles of the r.m.s normal and spanwise velocity components (figure 8) are maximum at the centre of the channel (as one would find in a Couette flow), but the streamwise component shows a clear minimum. Looking for an explanation in the budget of the streamwise Reynolds stress (figure 9), we find that indeed the shear production term is maximum at the center (due to the fact that the wall normal stress is maximum while the velocity gradient is fairly constant), but this production is significantly reduced by a negative turbulent transport term. Note again that a gradient diffusion model would give a positive contribution at the center. Another effect of the same order is the fact that the gravity production decreases towards the center, in accordance with the vertical

heat flux shown on figure 4.

The budget of vertical heat flux, which has a significant effect on other components through gravity effects, can be seen in figure 10. In the center of the channel, both velocity and temperature gradients make significant contribution through the production term, but near the wall this term becomes negative because of the change of sign of the velocity gradient. Still the vertical heat flux remains positive and is even maximum in the vicinity of the wall due to the joint effect of gravity production and, again, transport terms. The same comments as above can be made concerning the inadequacy of gradient diffusion modelling of the turbulent transport terms in the center of the channel. Note also that the dissipation term is non-zero throughout the channel due to the low Re number of this flow.

Last, and for completeness, the temperature variance and its budget are shown on figures 11 &12.

3. SECOND MOMENT CLOSURES

3.1 Current approaches

A variety of near-wall second moment closures have been proposed (see review of 9 models by So et al. [14]). Most of them use damping functions to force homogeneous models to comply with near wall turbulence features. A sound general tendency is to avoid the explicit use of the distance to the wall, e.g. Launder & Tselepidakis [15]. Besides, an extensive validation of this type of models in natural convection situations has been conducted by Hanjalic et al. [16].

An alternative to damping functions is the elliptic relaxation model of Durbin [2] by which features of (non-buoyant) near-wall turbulence can be satisfactorily reproduced by combining a simple homogeneous second moment closure with a nonlocal (elliptic) approach representing the wall blocking effect on the large eddies.

3.2 Triple correlations modeling

As will be shown below, the straightforward application of this model already yields fairly acceptable results. Most of the discrepancy was found in the central region of the channel where the transport terms in any second moment equation budget appear to play an important role and to behave, as previously noticed, in a particular manner. Usually triple correlations are modelled using a generalized gradient diffusion hypothesis (GGDH) such as in Daly and Harlow [17] :

$$R_{i\varphi\psi} \equiv \overline{u_i\varphi\psi} = -C_s \frac{k}{\varepsilon} \overline{u_i u_l} \frac{\partial \overline{\varphi\psi}}{\partial x_l} \quad \text{(where } \varphi \text{ and } \psi \text{ are any fluctuating quantities)} \qquad (5)$$

or in Hanjalic Launder [18] :

$$R_{i\varphi\psi} \equiv \overline{u_i\varphi\psi} = -C_s \frac{k}{\varepsilon} \left\{ \overline{u_l\psi} \frac{\partial \overline{u_i\varphi}}{\partial x_l} + \overline{u_l\varphi} \frac{\partial \overline{u_i\psi}}{\partial x_l} + \overline{u_i u_l} \frac{\partial \overline{\varphi\psi}}{\partial x_l} \right\} \qquad (6)$$

Unfortunately in the present natural convection case, this leads to wrong behaviour of transport terms as shown in figure 13 for R_{300}. Going back to triple correlation equations and accounting for production by mean temperature and velocity gradient, one can obtain (along the same lines as the ASM derivation) a little more complex algebraic model for triple correlations, called hereafter the

Algebraic Transport model (ATM) which reads as follows:

$$\begin{bmatrix} T_D & 0 & 0 & 2T_U & -2B & 0 & 0 & 0 & 0 & 0 & 0 & 0 & 0 \\ 0 & T_D & 0 & 0 & 0 & 0 & 0 & 0 & 0 & 0 & 0 & 0 & 0 \\ 0 & 0 & T_D & 0 & 0 & 0 & 0 & 0 & 0 & 0 & 0 & 0 & 0 \\ 0 & 0 & T_U & T_D & 0 & 0 & -B & 0 & 0 & 0 & 0 & 0 & 0 \\ 0 & 0 & 0 & T_\theta & T_{DT} & 0 & T_U & 0 & 0 & -B & 0 & 0 & 0 \\ 0 & 0 & 0 & 0 & 0 & T_{DT} & 0 & 0 & 0 & 0 & 0 & 0 & T_\theta \\ 0 & 0 & T_\theta & 0 & 0 & 0 & T_{DT} & 0 & 0 & 0 & 0 & 0 & 0 \\ T_\theta & 0 & 0 & 0 & 2T_U & 0 & 0 & T_{DT} & 0 & 0 & -2B & 0 & 0 \\ 0 & T_\theta & 0 & 0 & 0 & 0 & 0 & 0 & T_{DT} & 0 & 0 & 0 & 0 \\ 0 & 0 & 0 & 0 & 0 & 0 & 2T_\theta & 0 & 0 & T_T & 0 & 0 & 0 \\ 0 & 0 & 0 & 0 & 2T_\theta & 0 & 0 & 0 & 0 & T_U & T_T & 0 & 0 \\ 0 & 0 & 0 & 0 & 0 & 2T_\theta & 0 & 0 & 0 & 0 & 0 & T_T & 0 \\ 0 & 0 & 0 & 0 & 0 & 0 & 0 & 0 & 0 & 0 & 0 & 0 & T_D \end{bmatrix} \begin{bmatrix} R_{113} \\ R_{223} \\ R_{333} \\ R_{133} \\ R_{103} \\ R_{203} \\ R_{303} \\ R_{101} \\ R_{202} \\ R_{003} \\ R_{001} \\ R_{002} \\ R_{233} \end{bmatrix} = \begin{bmatrix} -2R_{13}D_{13} - R_{33}D_{11} \\ -R_{33}D_{22} \\ -3R_{33}D_{33} \\ -R_{13}D_{33} - 2R_{33}D_{13} \\ -R_{13}D_{30} - R_{30}D_{13} - R_{33}D_{10} \\ -R_{33}D_{20} \\ -R_{30}D_{33} - 2R_{33}D_{30} \\ 0 \\ 0 \\ -2R_{30}D_{30} - R_{33}D_{00} \\ 0 \\ 0 \\ 0 \end{bmatrix} \quad (7)$$

with :

$$\begin{cases} T_D = (k/\varepsilon) \\ T_{TD} = \left(\sqrt{(k/\varepsilon)\left(\overline{\theta^2}/\varepsilon_{\theta^2}\right)} \right) \\ T_T = \left(\overline{\theta^2}/\varepsilon_{\theta^2}\right) \end{cases} \quad \text{and} \quad \begin{cases} T_U = (\partial U/\partial z)^{-1} \\ T_\theta = (\partial \Theta/\partial z)^{-1} \\ B = g\beta \\ D_{ij} = \partial R_{ij}/\partial z \end{cases}$$

On the set of figures 13, the classical models for the turbulent transport terms appearing in the R_{11}, $R_{1\theta}$ and $R_{\theta\theta}$ budgets are actually in opposition to the DNS results in the central part of the channel. These are precisely the components that show a significant dip at the center. On the other hand using the ATM improves the predictions. Actually the major improvement is due to the velocity and temperature gradient production terms. Sensitivity of the results to the presence of buoyancy (B) terms can be considered as negligible since the amplitude of the profiles only change by a few percent. In addition, tests reported in [8], concerning the selection of the various time scales (either thermal or dynamical, or mixed) can make the maxima of the heat flux transport terms vary by a factor of nearly 50%, bringing them in better agreement with the DNS data when the geometrical average of dynamical and thermal time scales is used.

As could be expected, the new model improves the predictions of the second moments, essentially the dip in the R_{11}, $R_{1\theta}$ and $R_{\theta\theta}$ profiles (figure 14). This however has a negligible effect on the mean velocity and temperature profiles which were already quite well predicted. The same model was then applied to a second database at Ra =5.4 10^5 with similar agreement. Both databases are available electronically upon request.

4. CONCLUSION

Results of a direct numerical simulation of an infinite differentially heated vertical slot were obtained at Ra = 10^5 and compared straightforwardly with a second moment closure. This level of modelling is required by the presence of countergradient fluxes, but furthermore an algebraic third order closure was found necessary because of counter gradient turbulent transport terms which appear to mainly originate from the mean velocity and temperature gradient terms usually neglected in conventional transport models.

5. REFERENCES

1 T. J. Craft, B. E. Launder, (1991), Computations of impinging flows using second moment closures, 8th Symp. on Turbulent Shear Flows, Munich.

2 P. A. Durbin, (1993), A Reynolds stress model for near wall turbulence, JFM 249, pp. 465-498.

3 J. L. Lumley, (1978), Computational modeling of turbulent flows., Advances in applied mechanics, vol.18 .

4 N. Kasagi, Y. Tomita, A. Kuroda, (1992), "Direct numerical simulation of passive scalar field in a turbulent channel flow", ASME Journal of Heat Transfer, vol. 114, pp. 598-606.

5 S. L. Lyons, T. J. Hanratty, J. B. McLaughlin, (1991), "Direct numerical simulation of passive heat transfer in a turbulent channel flow", Int. J. Heat Mass Transfer, vol. 34, pp. 1149-1160.

6 R. J. A. Janssen, R. A. W. M. Henkes, C. J. Hoogendoorn, (1993), "Transition to time-periodicity of a natural convection flow in a 3D differentially heated cavity", Int. J. Heat Mass Transfer, Vol. 36, n°11, pp. 2927-2940.

7 S. Xin, (1993), "Simulations numériques de convection naturelle turbulente", Ph. D. thesis, Université de Paris XI, France.

8 R. Boudjemadi, (1995), Ph. D. thesis in preparation, Université de Paris XI, France.

9 C. M. Vest, V. S. Arpaci, (1969), "Stability of natural convection in a vertical slot", J. Fluid Mech. Vol. 36 part 1 pp. 1-16.

10 G. Grötzbach, M. Wörner, (1992), Analysis of second order transport equations by numerical simulations of turbulent convection in liquid metals, 5th International Topical Meeting on Nuclear Reactor Thermal Hydraulics, Salt Lake City.

11 H. Schmidt, U. Schumann, H. Volkert, (1984),"three-dimensional direct and vertorized elliptic solvers for various boundary conditions", DFVLR - Mitt. 84-15.

12 A. Chait, S. A. Korpela, (1989), "The secondary flow and its stability for natural convection in a tall vertical enclosure", J. Fluid Mech. Vol. 200 pp. 189-216.

13 J. Jimenez, P. Moin, (1991), "The minimal flow unit in near-wall turbulence", J. Fluid Mech. Vol. 225 pp. 213-240.

14 R. M. C. So, Y. G. Lai, H. S. Zhang, B. C. Hwang, "Second-order near-wall turbulence closures : a review", AIAA J., vol. 29, n° 11.

15 B. E. Launder, D. P. Tselepidakis (1991), "Progress and paradoxes in modelling near wall turbulence", 8th Symp. on Turbulent Shear Flows, Munich.

16 K. Hanjalic, "Achievements and limitations in modelling and computation of buoyant turbulent flows and heat transfer", 10th Int. Heat Transfer Conf., Brighton, U.K., 13-16 Aug. 1994.

17 B. J. Daly, F. H. Harlow, (1970), "transport equations of turbulence", The Physics of Fluids, Vol. B, pp. 2634-2649.

18 K. Hanjalic, B. E. Launder, (1976), "Contribution towards a Reynolds Stress closure for low-Reynolds number turbulence", J. Fluid Mech. Vol. 74 part 4 pp. 593-610.

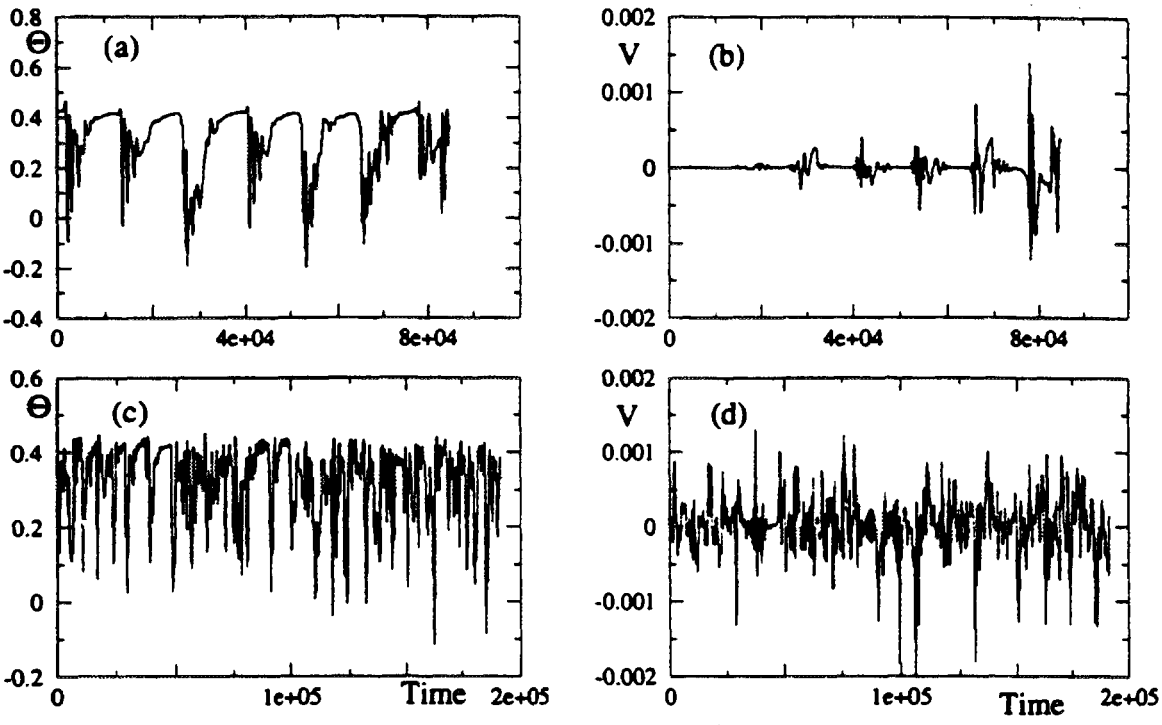

Fig 1: Time evolution. (a) & (b) $\Theta(=\Theta^b+\theta)$ and V(=v) quasi-periodic solutions. (c) & (d) Θ and V chaotic solutions.

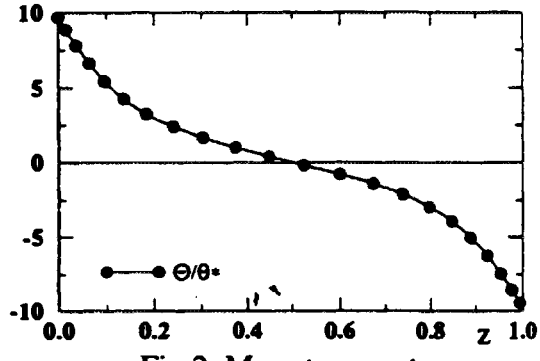

Fig 2: Mean temperature.

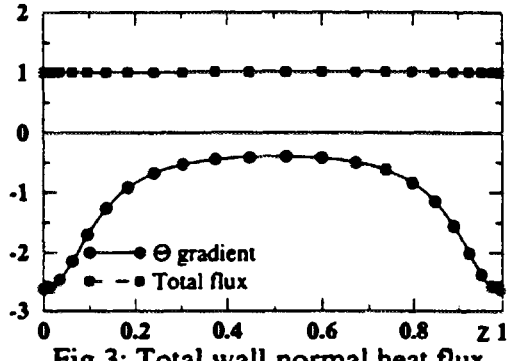

Fig 3: Total wall normal heat flux and mean temperature gradient.

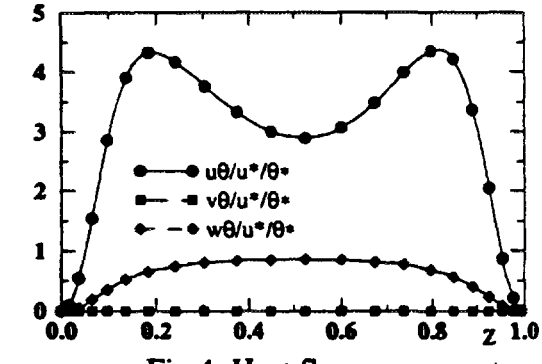

Fig 4: Heat flux components.

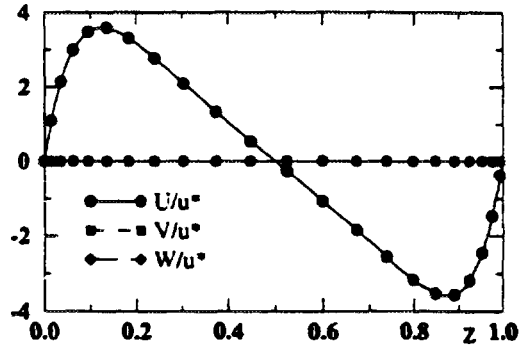

Fig 5: Mean velocity components.

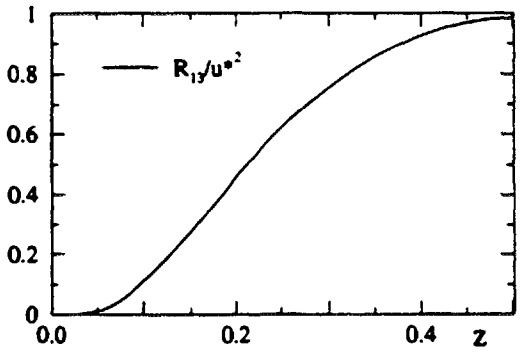

Fig 6: R_{13} profile

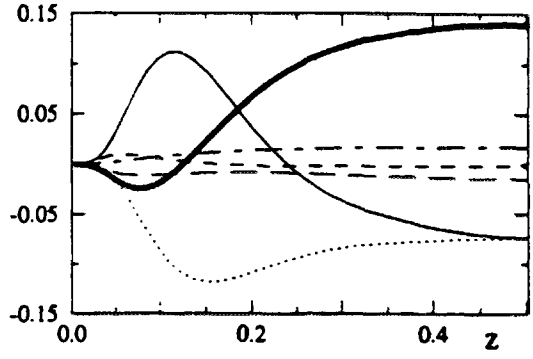

Fig 7: R_{13} budgets

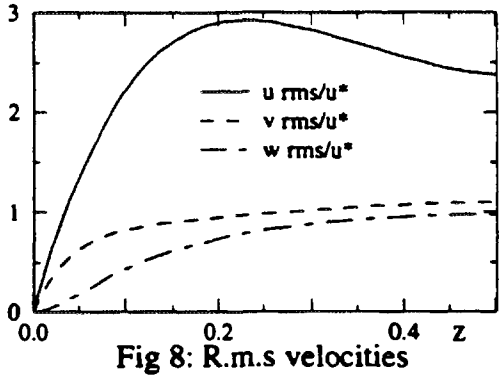

Fig 8: R.m.s velocities

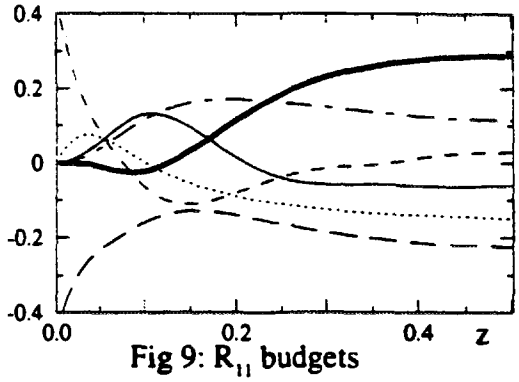

Fig 9: R_{11} budgets

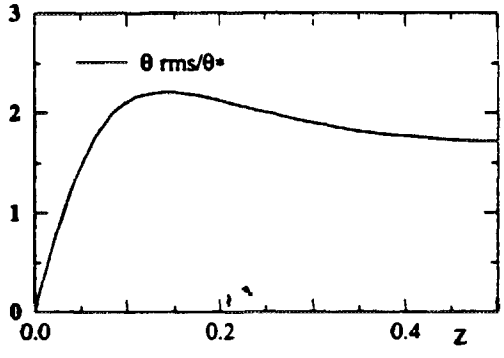

Fig 11: R.m.s temperature

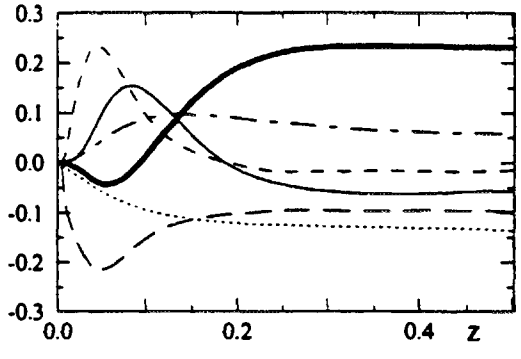

Fig 10: $R_{1\theta}$ budgets

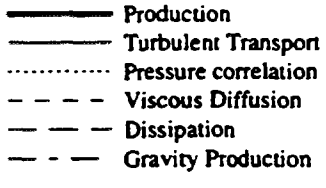

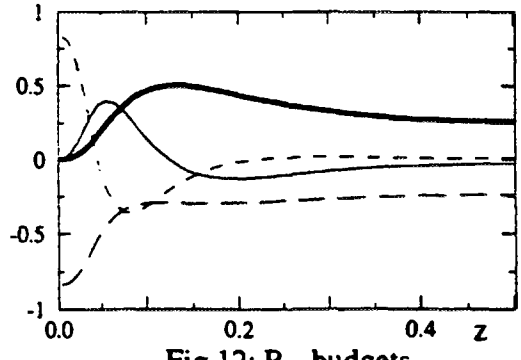

Fig 12: $R_{\theta\theta}$ budgets

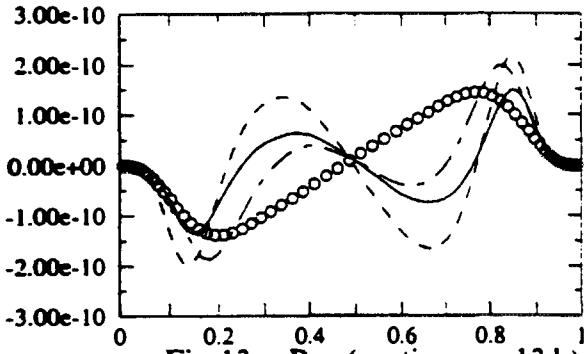

Fig 13.a: R_{113} (caption: see 13.b)

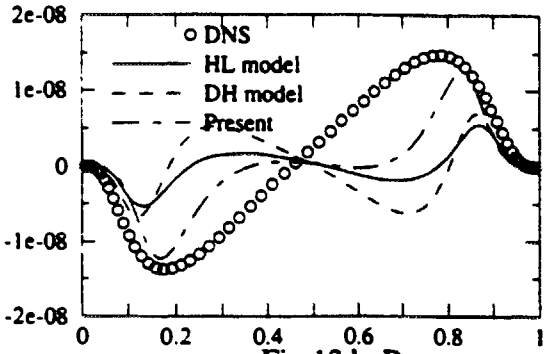

Fig 13.b: $R_{13\theta}$

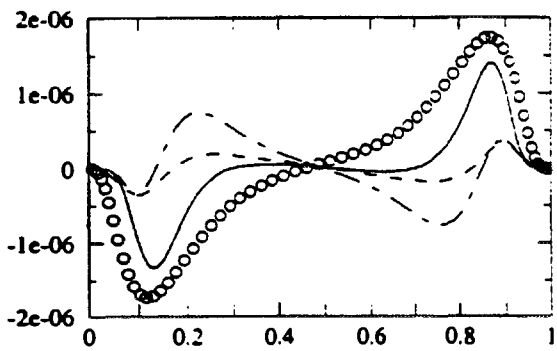

Fig 13.c: $R_{3\theta\theta}$ (caption: see 13.b)

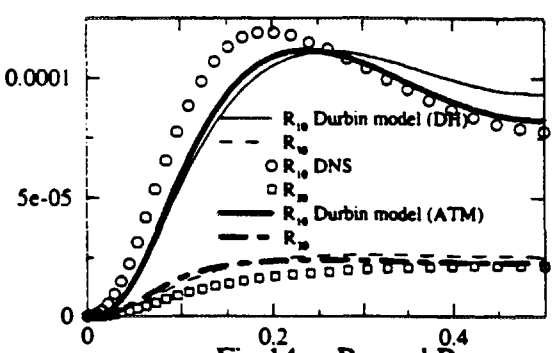

Fig 14.a: $R_{1\theta}$ and $R_{3\theta}$

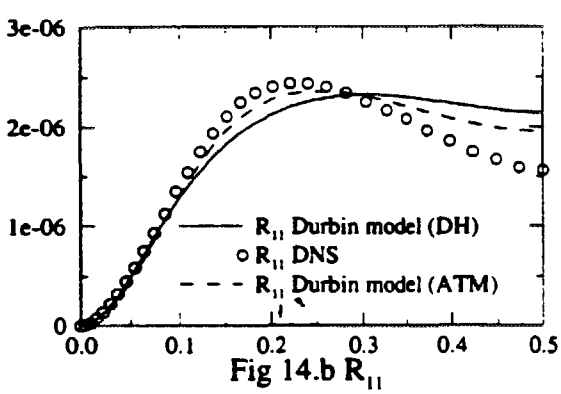

Fig 14.b R_{11}

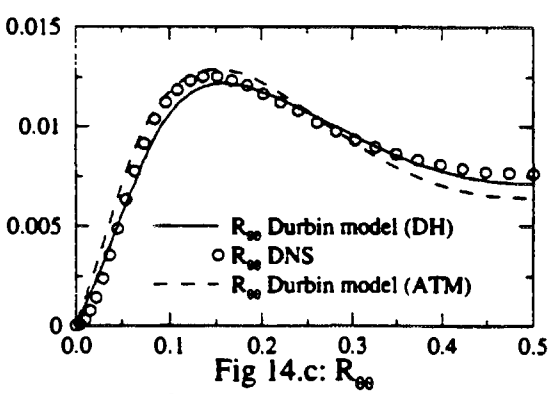

Fig 14.c: $R_{\theta\theta}$

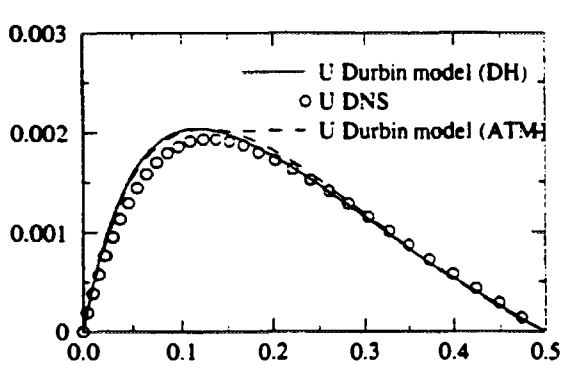

Fig 14.d: Mean velocity U

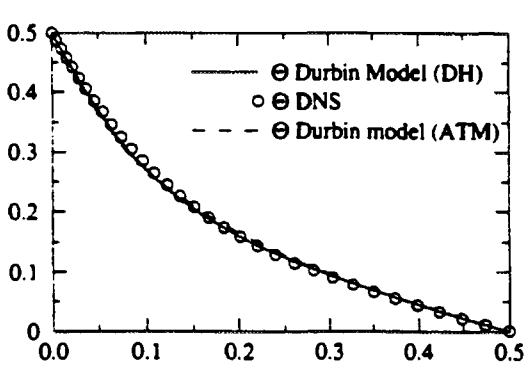

Fig 14.e: Mean temperature Θ